

Research article

***In-situ* formation of ZnO anchored silica: Sustainable replacement of conventional ZnO in SBR/NR blends**

Sreethu Thiyyanthiruthy Kumbalaparambil[✉], Ajay Haridas Chandaparambil[✉], Kinsuk Naskar^{*✉}

Rubber Technology Centre, Indian Institute of Technology Kharagpur, 721302 West Bengal, India

Received 18 July 2023; accepted in revised form 19 September 2023

Abstract. The global concern over zinc leaching into aquatic ecosystems has led researchers to seek ways to reduce zinc oxide (ZnO) content in rubber products. Conventional microsized ZnO, commonly used in the rubber industry, poses dispersion challenges due to its hydrophilic nature and micron size within the hydrophobic rubber matrix. Therefore, higher amounts of ZnO are added, elevating the risk to aquatic life. A promising alternative involves using highly dispersible ZnO with active zinc (Zn) centers instead of conventional ZnO. Another approach includes incorporating ZnO-anchored silica particles into the rubber matrix, which requires additional ex-situ fabrication. This study presents an innovative method where ZnO-anchored silica is generated in situ during the blending of styrene-butadiene rubber/natural rubber (SBR/NR). The study also evaluates the effectiveness of active, nano-sized, and octylamine-modified ZnO as activators compared to conventional ZnO, by introducing silica filler, octylamine-modified and high surface area ZnO anchor onto the silica surface, forming Si–O–Zn covalent bonds. This protective layer reduces filler aggregation and the Payne effect. Even with 60% less usage, these activators in the SBR/NR blend significantly enhance tensile strength (31.27%) and elongation at break (49.13%) compared to conventional ZnO. These results point towards the possibility of a cost-effective and sustainable replacement for conventional ZnO.

Keywords: sustainability, ZnO anchored silica, activator, kinetics, payne effect

1. Introduction

Zinc oxide (ZnO) is regarded as the most efficient activator due to its faster cure kinetics; by interacting with sulfur and accelerators, ZnO forms zinc polysulfide complexes that bond to rubber chains to produce a three-dimensional crosslinked structure [1, 2]. The ability of Zn²⁺ ions to form complexes is a crucial aspect of the activation mechanism [3]. It highly depends on its dispersion state in the rubber matrix, crystalline structure, surface area, and particle size [4, 5]. Traditionally, in rubber compounds, micron-sized conventional ZnO is being utilized. The inadequate dispersion of micro-sized conventional ZnO particles within the rubber matrix results in only a limited amount of ZnO being able to react effectively with other curing compounds. To compensate for this

limitation, a higher quantity of ZnO is typically added to rubber compounds, which raises significant environmental concerns due to its subsequent leaching during rubber products' production, application and disposal stages [6, 7]. It has shown detrimental effects on water quality and ecosystems, impacting various plants, invertebrates, and fish in freshwater/marine environments. Furthermore, excessive exposure to Zn poses a particular threat to aquatic organisms, disrupting their biochemistry [8]. In light of these environmental and ecological concerns, reducing the amount of ZnO in rubber compositions is imperative while maintaining desired performance levels [9, 10].

Various approaches have been proposed to address these concerns. Among them, the use of ZnO

*Corresponding author, e-mail: knaskar@rtc.iitkgp.ac.in
© BME-PT

nanoparticles was introduced first and gained significant interest because of the better dispersion in rubber matrix due to its small size, high surface area (7–10 m²/g.), and high surface-to-volume ratio, which lead to increased curing efficacy [11–17]. Yang and Xie [18] investigated the impact of particle size and surface area on the Zn²⁺ release ratios from Zn particles. Nano ZnO releases more Zn²⁺ than micro ZnO; the maximum ratios obtained were 85 and 60%, respectively. This is due to the nanoparticles' high surface-to-volume ratio, which provides an abundance of active zinc atoms on the surface. The same applies to active ZnO having a higher surface area with high Zn²⁺ ions accessibility. Active ZnO, with a surface area of 35 m²/g, offers substantially more reaction sites on the particle surface than conventional ZnO, which possesses a surface area of 4.5 m²/g [19–21]. The high availability of Zn²⁺ ions on its surface reduced the ZnO amount in rubber compounds. Recent studies explore the reduction of nano ZnO agglomeration tendency due to its smaller particle size with the surface modification of ZnO nanoparticles [22–26]. Qin *et al.* [27] modified nano ZnO with octylamine and the octylamine modifier prevented nanoparticle aggregation, resulting in a uniform dispersion of octylamine-modified ZnO nanoparticles in the rubber matrix. Since most studies were conducted on unfilled systems, the interaction between ZnO and the reinforcing filler remains unexamined.

Due to rising global concerns about emissions of greenhouse gases and climate change, silica-filled rubber compounds are gaining prominence [28]. The interaction between filler/filler and filler/polymer interaction primarily determines filler network structure. An essential criterion for developing highly reinforced rubber composites is the matrix's uniform distribution of filler particles. When mixed with non-polar elastomers, the polar surface chemistries of silica nanoparticles cause them to develop highly agglomerated structures. The utilization of silane coupling agents in silica/elastomer nanocomposites leads to a significant improvement in the dispersion of silica particles [29]. The cure activator ZnO also takes part in the dispersion of filler in the matrix. The surface silanol groups of silica are acidic and can, therefore, react with an alkali, such as ZnO. There are no extensive studies on the interaction of ZnO activators and fillers and how the type of ZnO affects the distribution of silica filler in rubber compounds. It has also proven to be a fascinating strategy to use

ZnO-anchored silica particles in rubber matrix, but this requires additional ex-situ fabrication of ZnO-anchored silica particles [1, 30].

The current study investigates the *in-situ* formation of ZnO-anchored silica particles during the processing. The study examined the effects of using different types of ZnO, including active, nano, and octylamine-modified ZnO, compared to conventional ZnO. With the inclusion of silica filler, the octylamine-modified ZnO and high surface area active ZnO were attached to the silica surface, forming covalent bonds as Si–O–Zn. This bonding process resulted in an extra protective layer on the surface of silica, which reduced the filler's aggregation and mitigated the Payne effect's occurrence. Fourier transform infrared (FTIR) spectroscopy and X-ray diffraction (XRD) analysis were performed to confirm the interaction between ZnO and silica particles.

These findings signify that the presence of highly reactive Zn²⁺ on the surface of ZnO enables the anchoring of ZnO onto silica particles without additional steps or chemical agents. Furthermore, it has been observed that this process improves the efficiency of rubber curing and reduces the required amount of ZnO by 60%, thereby exploring the potential for a cost-effective and sustainable alternative to conventional ZnO. Additionally, the mechanical and thermal properties of the blends were influenced by the type of sulphide linkage formation. This insight was gained by analyzing the influence of various ZnO on sulphide linkage formation using temperature scanning stress relaxation (TSSR) and thermogravimetric analysis (TGA) techniques.

2. Experimental details

2.1. Materials

Natural Rubber SVR3L grade, sourced from JK Fener Pvt. Ltd. in Mysore, India. The styrene-butadiene rubber (SBR) grade 1502 was purchased from Reliance Industries Pvt Ltd. in Mumbai, India. The styrene-butadiene rubber/natural rubber (SBR/NR) blend system was activated with four distinct vulcanization activators, including commercial ZnO (POCL, Thiruvallur, India), active ZnO (Transpek Silox Industry, Gujarat, India), nano ZnO (Nano Research Lab, Jharkhand, India), and functionalized ZnO (Tata Chemicals Ltd, Pune, India). Highly dispersible silica (HDS)(Zeosil), the reinforcing filler used in this study, was obtained from Solvay silica (Aubervilliers, France).

Table 1. Composition of SBR/NR blends filled with silica filler incorporating various ZnO activators.

Ingredients [phr]	C5BS [phr]	A2BS [phr]	N2BS [phr]	F2BS [phr]
Styrene-butadiene rubber (SBR)	70	70	70	70
Natural rubber (NR)	30	30	30	30
Conventional ZnO	5	–	–	–
Active ZnO	–	2	–	–
Nano ZnO	–	–	2	–
Functionalized ZnO	–	–	–	2
Stearic acid (SA)	2	2	2	2
Highly dispersible silica (HDS)	60	60	60	60
Bis(triethoxysilylpropyl)tetrasulfide (TESPT)	5.6	5.6	5.6	5.6
Hydroquinone (HQ)	1.0	1.0	1.0	1.0
Sulfur (S)	1.5	1.5	1.5	1.5
Tetramethylthiuram disulfide (TMTD)	0.5	0.5	0.5	0.5
Cyclo benzyl sulfenamide (CBS)	1.2	1.2	1.2	1.2

phr: parts per hundred rubbers

2.2. SBR/NR blend mixing

The blend has been mixed in two steps. All the additives, except curatives termed as master batch, have been added to the Brabender internal mixer (Brabender GmbH, Duisburg, Germany). Throughout the mixing period, the temperature was kept at 140 °C. During the initial mixing stage, the rpm addition of rubber and activators was set at 30. After adding the remaining ingredients for compounding, the mixing speed was increased to 60 rpm, and the total mixing time was set to 4.5 min. The final batch containing the curatives mixed in the lab two-roll mill. The blend composition is shown in Table 1. Throughout the text, the blend contains 5 phr conventional ZnO called C5BS. The blend comprises active, nano, and functionalized ZnO called A2BS, N2BS, and F2BS. Here, 2 stands for 2 phr of ZnO addition, and S stands for the reinforcing filler, highly dispersible silica.

2.3. Instrumentation and characterizations

The curing characteristics of the SBR/NR blends were monitored by subjecting them to a moving die rheometer (Monsanto Rheometer (MDR 2000), Akron, USA) at 150 °C for 45 min under an oscillation angle of 3 arcs. To determine the cure kinetics, we cured the rubber mixtures at three different temperatures for 45 min: 140, 150, and 160 °C. The activation energy and rate constant were calculated using the Arrhenius equation for first-order kinetics and a nonlinear curve fitting according to the Kamal-Sourour model. The Flory-Rehner equation was employed to determine the crosslink density. A

comprehensive description of the procedure can be found in the supporting information section.

X-ray diffraction (XRD) and Fourier transform infrared spectrophotometry (FTIR) were employed to analyze the blend structures. XRD analysis was performed using a Bruker D8 Advance XRD instrument (Germany), utilizing Cu K α (wavelength = 1.54 Å) radiation. The XRD measurements covered an angular range of 20° to 90° with a step size of 0.04°. FTIR (Nicolet 6700, M/S thermo fisher scientific instruments, Madison, USA) in attenuated total reflectance (ATR) mode was used to detect the functional groups in the composites. The spectra were recorded between 400 and 4000 cm⁻¹ with a 16 scan and a force gauge setting 32. Using a thermogravimetric analyzer (Shimadzu TGA 50, Columbia, USA), mixtures were subjected to thermogravimetric analysis (TGA). Under a nitrogen atmosphere, samples of approximately 8 mg each in an alumina crucible were heated at 10 K/min.

To comprehend the blends thermomechanical characteristics, we carried out temperature scanning stress relaxation measurements using the TSSR-Tester (Brabender GmbH, Duisburg, Germany). The specimen shaped like a dumbbell (ISO 527, Type 5A) was cut from the molded sheet. The sample was placed in an electrically heated chamber and subjected to a 50% initial strain for 2 h at 23 °C. This was carried out so that short-term relaxation processes could dissipate. Then, a nonisothermal measurement up to 200 °C was carried out at a 2 K/min heating rate until the sample ruptured or stress relaxation was complete. Using stress-temperature curves derived from

TSSR testing was employed to assess crosslink density. This was achieved by calculating the initial slope of the curves using a modified Neo-Hookean equation.

The blend's tensile and tear properties were measured at room temperature using a Hiosk-Hounsfield universal testing machine (Surrey, England) (with a 10 kN load cell and 500 mm/min crosshead speed). Using ASTM D412 die C the specimens were cut from the moulded tensile sheet. To comply with ASTM D573 standards, accelerated aging was conducted using a forced air circulating oven (Blue M Electric, model N^o F0 712, Blue Island, Illinois, USA). The aging process was performed at 70 °C for one week. After aging, the mechanical properties of the specimens were evaluated following a 40 h conditioning period at 23 °C and 50% relative humidity to ensure thermal equilibrium. The tensile strength, elongation at break, and modulus of aged samples were evaluated compared to those of unaged samples.

Temperature-sweep tests using an Eplexor 2000 instrument from Gabo Qualimeter (Netzsch, Geratebau GmbH, Selb, Germany) determined the rubbery nature of the samples. The sample of size 35×10×2 mm was cooled to –80 °C and then heated to 80 °C at a rate of 2 K/min and a constant frequency of 10 Hz.

The viscoelastic properties of the prepared rubber mixture were evaluated using a Rubber Process Analyzer (RPA) (RPA 2000, Alpha Technologies, UK). For the strain sweep study, the temperature was held constant at 100 °C. Adjusting the strain from 0.05 to 100% while maintaining a frequency of 0.33 Hz. By calculating the difference between the elastic moduli at low strain (G_0') and high strain (G_{∞}'), the Payne effect was determined from the RPA. This method was used to evaluate filler-filler interactions in compounds; the greater the Payne effect, the greater the filler-filler interaction.

The analysis of filler dispersion in the composites was conducted using transmission electron microscopy (TEM) with a JEM 2100F (Jeol, Japan) as well as scanning electron microscopy (SEM) using a Merlin microscope (Carl Zeiss SMT, Germany). The TEM instrument operates with a 120 kV electron beam at an accelerated voltage. Before the test, the rubber compounds were prepared with an ultramicrotome. After cryo fracturing in liquid nitrogen and overnight drying at 60 °C, SEM samples were prepared.

3. Results and discussion

3.1. Effect of various activators on the cure characteristics

Table 2 summarises the cure parameters such as highest torque (M_H), lowest torque (M_L), delta torque ($M_H - M_L$), optimum cure time (T_{c90}), scorch time (T_{s2}), and the cure rate index (CRI), obtained from the rheocurve of silica-filled SBR-NR blends containing conventional, active, nano and functionalized ZnO. Figure 1 shows the acquired rheocurve and crosslink density of the SBR/NR blends. Octylamine-modified F2BS exhibited the lowest cure time among all blends. It is possible that octylamine, which raises basicity and speeds up the vulcanization process, is the cause of the F2BS low cure time and higher cure rate index [31, 32]. The highest torque (M_H) of F2BS modified with octylamine was reduced, suggesting that blends of octylamine-modified ZnO with SBR/NR blend have a lower degree of rubber reticulation [27].

Blends N2BS and A2BS had a high T_{c90} and the low (CRI) results from the extended duration needed for chelate formation at high Zn ions concentration, which was enabled by the smaller particle size and larger surface area of nano and active ZnO [5, 33].

However, the silanol or hydroxyl groups on the surfaces of silicas make them acidic and polar. Due to this, cure rates are slow and cure times are higher when compared to carbon black-filled blends inferred from our previous study. Notably, the silica-filled rubber vulcanizates exhibited a substantial delta torque ($M_H - M_L$), reflected in the greater crosslink determined from swelling study densities (Table 2; Figure 1b). Since TESPT, a silane compound containing sulfur, was used as a coupling agent, the tetrasulfide groups in TESPT caused the silica particles to interact with the rubber chains. Consequently, additional monosulfidic crosslinks formed in addition to those produced by elemental sulfur [34]. In silica-filled blends, N2BS had the highest delta torque and a similar value to C5BS blend among all the batches and F2BS exhibited the lowest delta torque value with a

Table 2. Cure characteristics of SBR/NR blends filled with silica fillers cured at 150 °C.

Entry	M_L [dN·m]	M_H [dN·m]	$M_H - M_L$ [dN·m]	T_{s2} [min]	T_{c90} [min]	CRI [min ⁻¹]
C5BS	6.67	34.45	27.78	2.22	15.92	7.30
A2BS	7.19	33.95	26.76	2.05	17.50	6.47
N2BS	6.74	34.67	27.93	2.08	19.21	5.84
F2BS	3.67	22.98	19.31	1.32	7.71	15.65

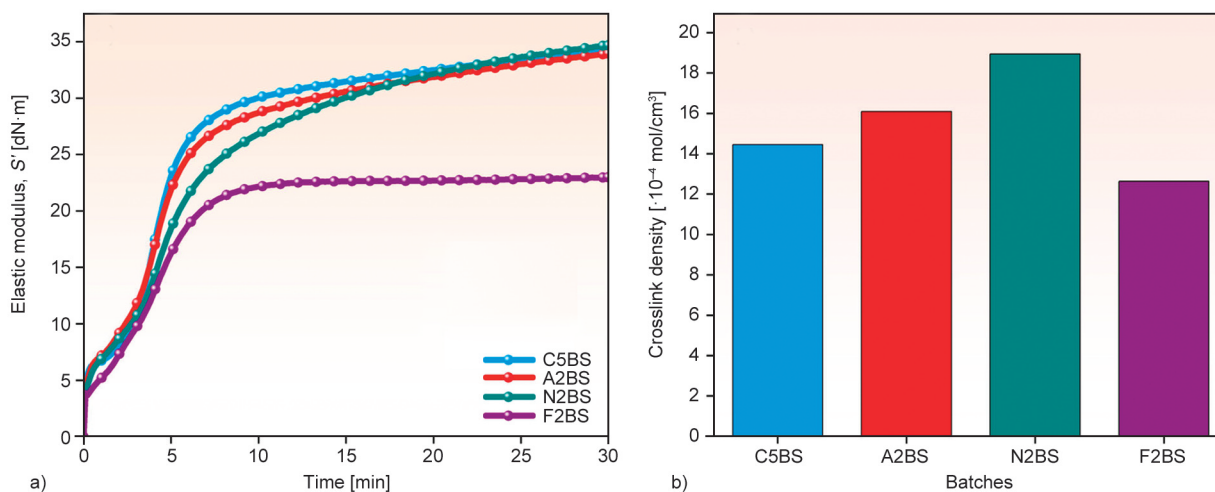


Figure 1. a) Time–elastic modulus curve, b) crosslink density measured from a swelling method using Flory Rehner equation.

30% reduction in the value. These results correlated with the crosslink density obtained in Figure 1b.

Activation energy

Cure kinetics tests were done on SBR/NR blends to see how different ZnO concentrations affected the activation of sulfur vulcanization. Analyzed the kinetic constant (k) and activation energy (E_a) of the SBR/NR blends using cure data obtained at 140, 150, and 160 °C. The Kamal-Sourour reaction model was used for kinetic analysis. The curing of rubber compounds has been explained using the Kamal-Sourour reaction model, which incorporates autocatalytic characteristics with an n^{th} -order reaction model [35, 36]. Equation (1) serves as the basis for the Kamal-Sourour reaction model, capturing the n^{th} -order reaction component with the first-rate constant (k_1) and exponent (n) and the autocatalytic contribution to the reaction with the second-rate constant (k_2) and

exponent (m). Every kinetic constant follows the Arrhenius equation (Equation (1)):

$$\frac{d\alpha}{dt} = (k_1 + k_2\alpha^m)(1 - \alpha^n) \quad (1)$$

By fitting above Equation (1) to the slope of the graph between $d\alpha/dt$ and α , the rate constant k can be determined. The activation energy was then determined by plotting $\ln k$ vs. $1/T$ (Figure 2a). It adheres to the Arrhenius equation (Equation (2)), which relates the rate constant (k) to the pre-exponential factor (A), activation energy (E_a), universal gas constant (R), and temperature (T) in Kelvin. The obtained activation energy is shown in Figure 2b:

$$k = A e^{\frac{-E_a}{RT}} \quad (2)$$

The activation energy of the vulcanization reaction can serve to validate the efficiency of the activator

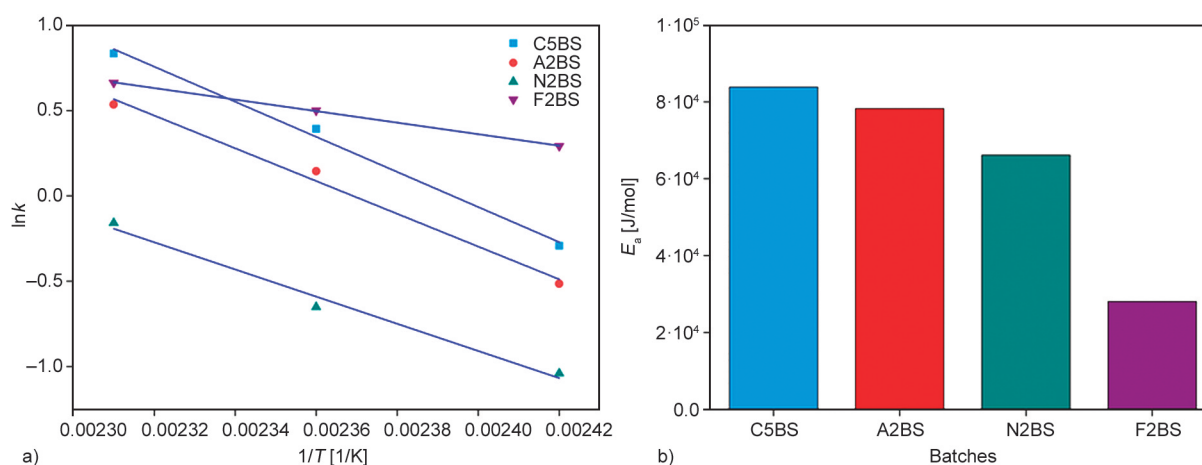


Figure 2. a) $\ln k$ vs. $1/T$ plot and b) obtained activation energy.

employed in the rubber formulation. The octylamine modified ZnO accelerates the vulcanization of rubbers by catalyzing the formation of a more active sulfurating agent due to the presence of amine on the surface. Consequently, the apparent activation energy of F2BS decreases. Figure 2b shows which F2BS had the lowest activation energy. This suggests that the F2BS vulcanizes more quickly in SBR/NR blends, consistent with the CRI in Table 2.

3.2. Characterizations-interfacial interaction of silica-filled SBR/NR blend with various ZnO

FTIR and XRD analysis

FTIR analysis was done on the four blends to investigate how ZnO interacted with the silica surface and stearic acid. C5BS, A2BS, N2BS, and F2BS, ATR-FTIR spectra were performed in the 400–4000 cm^{-1} range. The zoomed region of the FTIR spectra from 750 to 1050 cm^{-1} is displayed in Figure 3a. The peak at 954 cm^{-1} , attributed to the Si–OH stretching

vibration, undergoes a distinct transformation within all blend compositions. Notably, the peak's position shifts to a higher frequency range of 963–965 cm^{-1} , assuming a shoulder-like appearance, and concurrently, its intensity follows an ascending order of F2BS > A2BS > N2BS > C5BS (Figure 3a). Drawing parallels with previously documented spectra of ZnO–SiO₂ composites as found in the literature, this alteration is likely a consequence of the concurrent presence of Si–OH and symmetric Si–O–Zn stretching modes. This observation supports the proposition of covalent bonding between the surface silanol group filler and the activator ZnO particles [37–39]. This confirms the increased formation of Si–O–Zn bonds even during the ex-situ mixing of rubber compounds in the Brabender mixer.

Upon the interaction between ZnO and stearic acid, prominent peaks at 1538 and 1398 cm^{-1} were detected (Figure 3b), signifying the asymmetric and symmetric stretching of COOH groups linked to zinc centers within the Zn stearate framework [40]. The

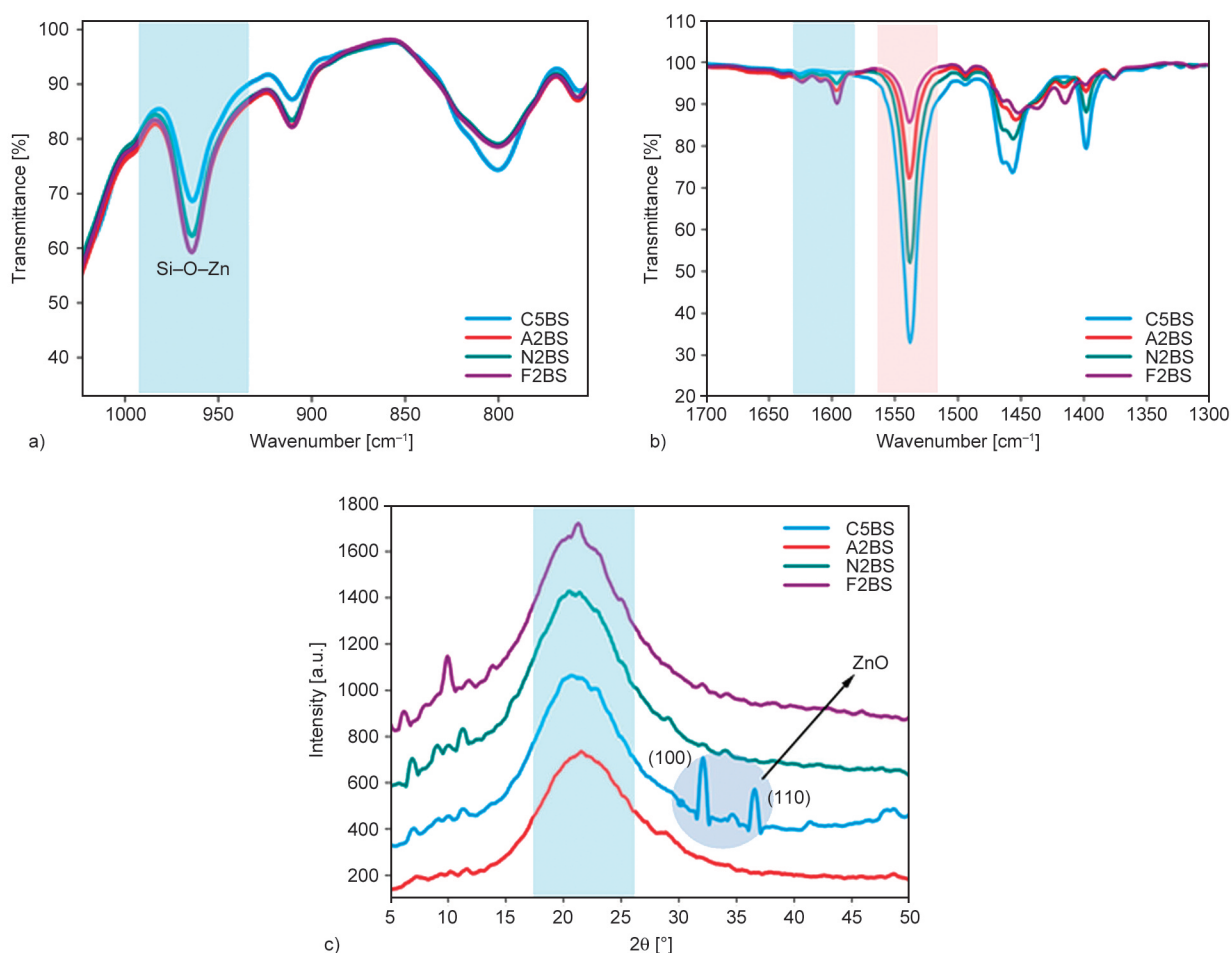


Figure 3. FTIR spectroscopy of C5BS, A2BS, N2BS and F2BS a) at zoomed wavelength of 1050–750 cm^{-1} , b) at zoomed wavelength of 1700–1300 cm^{-1} , c) XRD diffraction spectra of C5BS, A2BS, N2BS and F2BS.

interaction of ZnO-anchored silica particles with the stearic acid, especially within the F2BS and A2BS blends, showed a reduction in the intensity of the zinc stearate peaks. New peaks emerged at 1595, 1609, and 1624 cm^{-1} , accompanied by vibrations at 1415 cm^{-1} , with the order of intensity being F2BS > A2BS > N2BS > C5BS. These phenomena are believed to be associated with the formation of distinct surface zinc complexes due to the interaction of ZnO-anchored silica with stearic acid, as discussed by Ikeda *et al.* [41] and Mostoni *et al.* [40] that the spectral characteristics of ZnO/SiO₂ nanoparticles suggest the existence of bridging bidentate-coordinated zinc/stearate complexes in a dinuclear arrangement. Each stearic acid molecule links two zinc centers in this configuration, maintaining a Zn:SA molar ratio of 1:1. This arrangement results in two vacant positions on each Zn(II) site, potentially available for additional ligand binding.

Due to the silica's acidic surface silanol groups, an alkali like ZnO can react with them. Active ZnO, which had more readily available Zn²⁺, rapidly reacted with the silica surface to form the covalent bond Si–O–Zn, protect the silica particles with a layer, and reduce filler aggregation. Similarly, as demonstrated in Figure 9, octylamine-modified ZnO formed Si–O–Zn bonds and had a stronger affinity for the silica filler in F2BS due to its presence of an amine group in the surface of ZnO, making it more attracted to the silica surface and forming high-intensity Si–O–Zn bonds. Nano ZnO having a lower surface area (7–10 m^2/g) than the active ZnO (35 m^2/g) and a higher surface area than the conventional ZnO (4.5 m^2/g) make Zn²⁺ ions availability less compared to active and more compared to conventional ZnO. Figure 3c represents the XRD pattern of C5BS, A2BS, N2BS and F2BS. In the case of C5BS, the intensity of the peaks 2θ at 31.6° and 36.11°, which represent the (100) and (101) diffractions of ZnO, respectively, is visible because the micron-sized ZnO particles it contains reduced dispersion, allowing for the visualization of unreacted ZnO particles. The non-crystalline silica is characterized by the diffraction peak 2θ at 22.5°.

3.3. Temperature scanning stress relaxation of highly dispersible silica filled SBR/NR blends with various ZnO activator systems

The thermal stability of the elastomer network is an essential attribute of rubber vulcanizates. As

temperature increases, the thermal degradation of the rubber network is often accompanied by a substantial reduction in stress. To better understand the impact of different ZnO activators on the thermal stability of SBR/NR blends, temperature scanning stress relaxation (TSSR) experiments were conducted by observing the non-isothermal relaxation behavior as a function of temperature. The temperature at which crosslink cleavage or scission of the main chains occurs is indicated by significant peaks appearing in the relaxation spectrum. Each peak simultaneously reflects a relaxation mechanism. Figure 4 depicts the stress as a function of the temperature and the relaxation spectra of SBR/NR blends with varying ZnO activators.

In silica-filled SBR/NR blends, nano ZnO-loaded N2BS showed the highest stress, followed by A2BS and C5BS (Figure 4b), justifying the cure parameters obtained as N2BS had the highest delta torque among all the blends. F2BS with functionalized ZnO had the lowest stress value at constant strain magnitude. The higher stress value of N2BS and lower stress of F2BS is due to the higher crosslink density of N2BS and lower crosslink density of F2BS [42]. N2BS had the highest crosslink density among all other blends, and F2BS had the lowest. The change of stress with the temperature of silica-filled blends is shown in Figure 4. The reduction in relaxation stress with an increase in temperature was linked to the molecular mobility process, which was more pronounced for N2BS the reduction in relaxation stress with an increase in temperature was more pronounced for N2BS; it had the highest stress than C5BS, A2BS, and F2BS. The C5BS and N2BS exhibited a comparable temperature-dependent stress relaxation response and the lowest was observed for F2BS. From Figure 4a, the thermal stability of the blends can be accessed from T_{10} and T_{50} temperatures at which the stress of the blend has reduced by 10 and 50% obtained values were listed in Table 3.

The initial stress decay with temperature was observed, and A2BS had the highest, around 104 °C. In the case of C5BS, the T_{10} was at a lower temperature of 79 °C. N2BS reported T_{10} at 89 and 87 °C for F2BS were shown. The higher thermal stability was observed for A2BS due to its high surface area and the presence of more reactive Zn sites; its T_{50} was reported at 172 °C whereas C5BS had a similar thermal stability and T_{50} value around 171 °C due to the presence of high ZnO content (5 phr) in the respective blend.

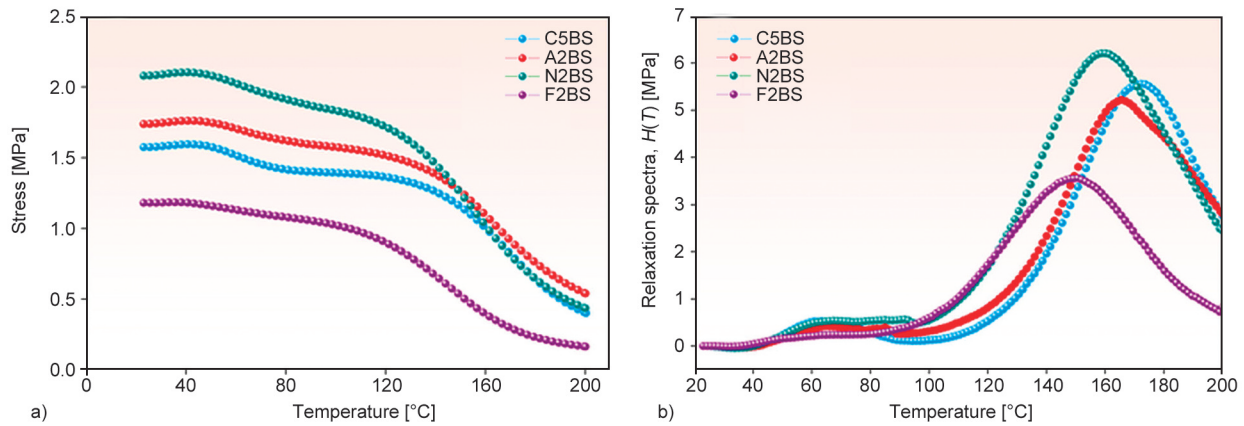


Figure 4. Non-isothermal stress relaxation test a) stress vs. temperature of HDS-filled SBR/NR blends with various ZnO as activators, b) relaxation spectra vs. temperature curve of HDS-filled SBR/NR blends containing various ZnO as activators.

Table 3. Degradation temperature obtained from the TSSR study.

Batch	T_{10} [°C]	T_{50} [°C]
C5BS	79.8	171.7
A2BS	104.6	172.7
N2BS	89.5	159.2
F2BS	87.2	145.3

N2BS shown T_{50} at 159°C and F2BS at 145°C shows the least thermal stability among all blends. The stress vs. temperature curve and the relaxation spectra vs. temperature are both shown in Figure 4. The relaxation spectrum $H(T)$, which is obtained from the stress vs. temperature curve, is obtained by differentiating the non isothermal relaxation modulus $E(T)$ with respect to temperature (T), as shown in Equation (3) [43]:

$$H(T) = -T \left(\frac{dE(T)}{dT} \right) \quad (3)$$

The peak around 110–150°C indicates the decomposition of polysulfidic linkages, here F2BS exhibited a peak below 150°C confirming that the presence of octylamine in the functionalized ZnO enables the faster curing and forming of the polysulfide linkages rather than di and monosulfidic. C5BS, A2BS and N2BS degradation peaks shifted to a higher temperature and showed a peak above 160°C confirming the presence of mono and disulfide linkages [44]. In the case of conventional ZnO-filled C5BS showed a prominent peak at 174°C. for A2BS 166, and 159°C for N2BS, respectively; the F2BS peak was seen at a lower temperature of about 149°C.

The stress of SBR/NR blends slightly increased in the 23–40°C temperature range, as shown in Figure 4a. Entropy effects inherent to rubber vulcanizates are responsible for this. Furthermore, the crosslink density in rubber vulcanizates is represented by this area (23–40°C) of the stress-temperature curve. Observing that stress-temperature graphs derived from the TSSR test were employed to assess crosslink density through the modified Neo-Hookean Equation (4) applied to the initial slope of the curves [44]:

$$\sigma = \nu RT \left(\left(\frac{\lambda}{1 + \alpha(T - T_0)} \right) - \left(\frac{\lambda}{1 + \alpha(T - T_0)} \right)^{-2} \right) \quad (4)$$

where σ represents stress, R stands for the universal gas constant, and α represents the thermal expansion coefficient, corresponding to a value of $2.4 \cdot 10^{-4} \text{ K}^{-1}$. The extension ratio, denoted as λ , is the ratio of the final length l to the initial length l_0 . T is the temperature in Kelvin.

The comparison of crosslink density obtained from TSSR and swelling study has been plotted in Figure 5, and it shows a positive correlation with the crosslink density obtained from the swelling study, as depicted in Figure 1b. The crosslink density of all the blends obtained from the TSSR experiment was lower than the one obtained from the swelling study. The resemblance in the crosslink density of blends derived from TSSR and swelling analysis demonstrates a consistent trend in the delta torque values. This suggests that the primary cause of torque development during vulcanization is the creation of crosslinks within the rubber matrix [45].

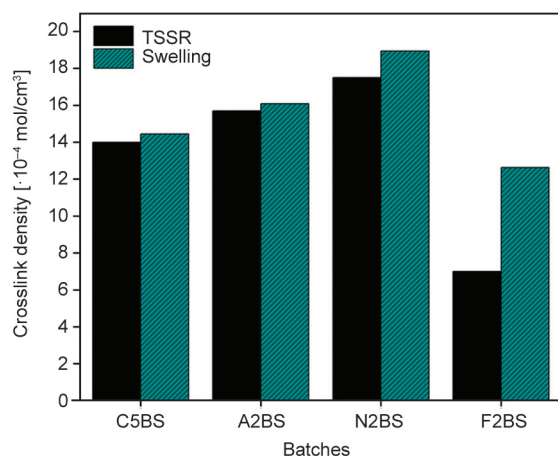


Figure 5. Crosslink density comparison between swelling and TSSR study of HDS-filled SBR/NR blends with various ZnO as activators.

3.4. Thermogravimetric Analysis (TGA)

The effect of the type of ZnO thermal stability on the silica-filled SBR/NR was investigated using the thermogravimetry (TG) technique and their derivative thermogravimetric (DTG) analysis. As seen in Figure 6a, the conventional ZnO-loaded C5BS had a little more residual weight after degradation than the other batches containing 2 phr of ZnO. This is due to the higher ZnO (5 phr) content of C5BS. The TG curves of all the samples under investigation primarily showed two degradation steps, as seen in the DTG curve (Figure 6). The rubber blend's plasticizer and volatile components degraded in the initial stage of degradation at around 370–400 °C. As can be seen, the degradation of SBR and NR caused most weight losses for all blends to occur between 420 and 480 °C. In Figure 6b, the degradation temperatures

of C5BS, A2BS, and N2BS are 461.67, 461.89, and 461.59 °C, respectively. It was nearly the same temperature range and demonstrates that the higher thermal stability of active ZnO and nano ZnO at 2 phr loading increases the thermal stability of the blend to the same level as conventional ZnO at 5 phr loading. The large dispersion of nanoparticles in the polymer matrix impeded the free radical's ability to diffuse, which delayed the degradation of rubber compounds. Additionally, ZnO nanoparticles' high heat capacity and thermal conductivity made them effective heat sinkers, absorbing more heat than the rubber matrix could hold onto, which increased the composites' thermal stability. Blends of A2BS and N2BS showed shifts to higher temperatures in their characterization temperatures due to their excellent dispersion in the matrix.

3.5. Dynamic mechanical analysis

The dynamic mechanical performance of the SBR/NR blends was analyzed over the temperature range of –80 to 80 °C. Figure 7 shows the comparative study of storage modulus and loss factor vs. temperature of silica-filled SBR/NR blends with various ZnO activators. The $\tan \delta$ vs. temperature at 0 °C predicted wet skid, and the $\tan \delta$ vs. temperature at 60 °C estimated rolling resistance and obtained values are listed in Table 4 [46]. A lower $\tan \delta$ value indicated better fuel efficiency and lower rolling resistance at 60 °C. Better wet traction was suggested by a higher $\tan \delta$ value at 0 °C. Change in traction was 0.6 and 1.1% lower for F2BS and A2BS than C5BS, which is negligible, and for N2BS, it was a 10% difference. The rolling resistance change was not in positive

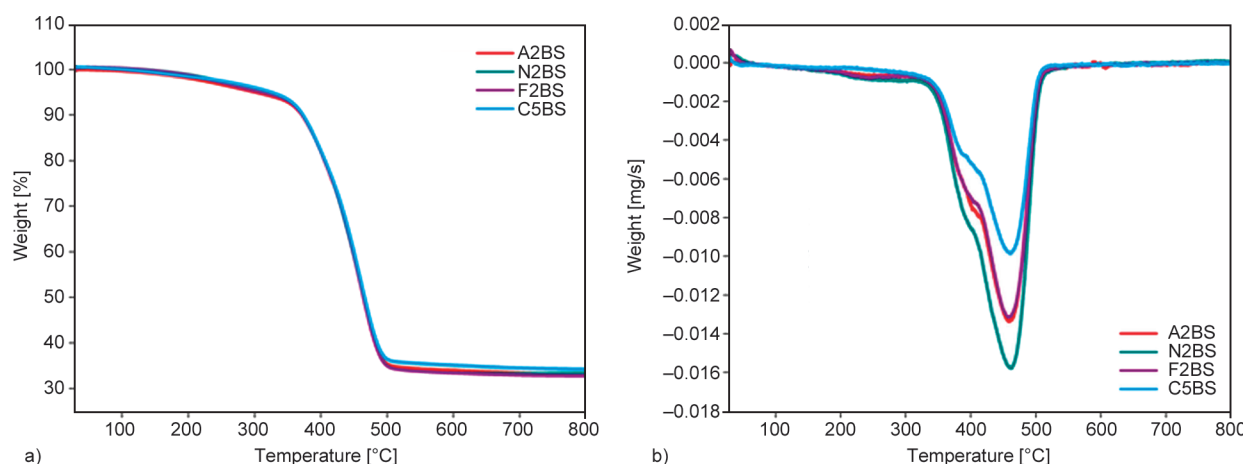


Figure 6. a) TGA curve of HDS-filled SBR/NR blends with various ZnO as activators, b) DTG plot of HDS-filled SBR/NR blends with various ZnO as activators.

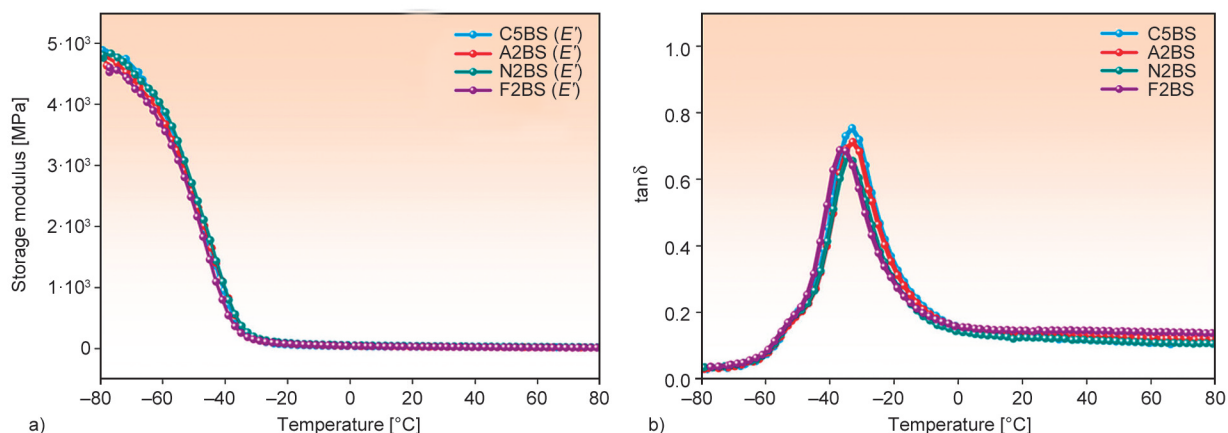


Figure 7. Dynamic mechanical analysis SBR/NR blends with various ZnO: a) storage modulus vs. temperature curve, b) $\tan \delta$ vs. temperature curve.

Table 4. Traction and rolling resistance obtained from dynamic mechanical analysis.

SBR/NR Blend	Traction ($\tan \delta$ at 0 °C)	Rolling resistance ($\tan \delta$ at 60 °C)
C5BS	0.1597	0.1078
A2BS	0.1579	0.1218
N2BS	0.1433	0.1095
F2BS	0.1586	0.1412

association for F2BS and A2BS increase in 30 and 12% compared to C5BS; for N2BS, it was a 1.4% increase in the $\tan \delta$ at 60 °C value.

The silica-filled blends showed no significant changes in the wet skid and rolling resistance in A2BS, N2BS, and F2BS compared to C5BS. Obtained rolling resistance and wet skid were in line with the value obtained for C5BS, thereby ensuring the reduction of ZnO is possible without affecting its main magic triangle properties of the tyre obtained from the dynamic mechanical analysis.

3.6. Payne effect interpretation of SBR/NR blends with various ZnO systems

Figure 8 depicts the RPA curve of storage modulus vs. strain and the resulting Payne effect obtained from the strain sweep analysis in the strain region of 0.5 to 100%. Here, we explore the Payne effect in silica-filled blends with various ZnO activators. The filler’s dispersion in the matrix significantly impacts the rubber blend mechanical performance. The Payne effect and SEM were used to analyze the dispersion state of blends. The storage modulus (G') of the rubber matrix reinforced with the silica filler increased as the strain increased, and the extent of this change under a final strain and initial strain was regarded as the Payne effect. The Payne effect can be resolute as $\Delta G = (G_0' - G_{\infty}')$. G_0' belongs to the storage modulus at the lowest strain, and G_{∞}' is the storage modulus at the highest operating strain (at 100% strain) [47–49]. A lower Payne effect value indicates better

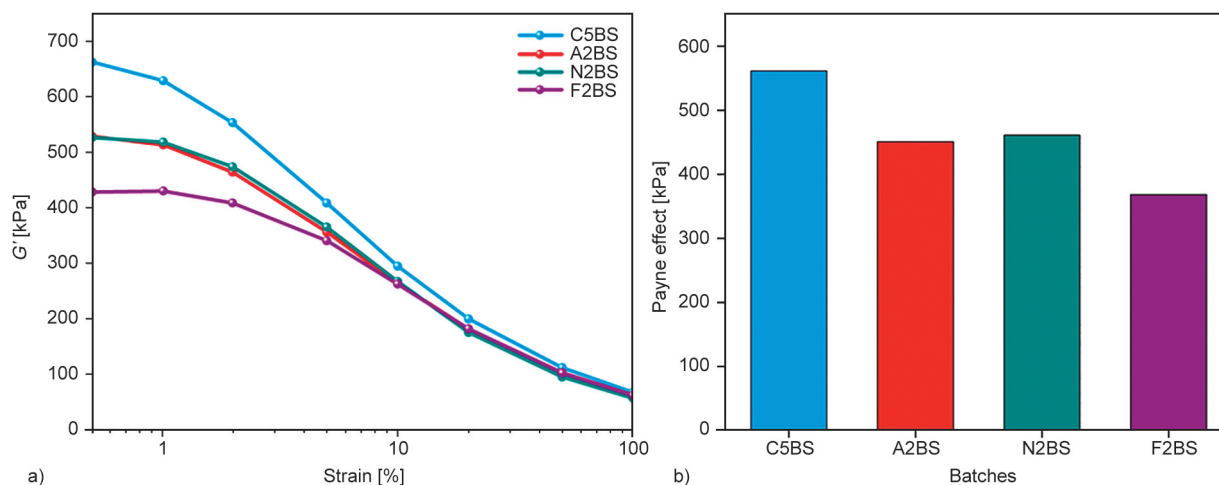


Figure 8. a) Strain sweep curve of ZnO in SBR/NR blends filled with highly dispersible silica, b) Payne effect in silica-filled blends.

filler dispersion, hence good polymer-filler interaction [50–52].

The F2BS blend containing octylamine-modified ZnO shows the lowest Payne effect. The octylamine-modified ZnO is known to improve the dispersion in thin film transistors [53]. Qin *et al.* [27] explored the octylamine-modified ZnO in NR and SBR matrix and found that the agglomeration has reduced and showed a better dispersion of Zn nanoparticles in the rubber matrix. Octylamine-modified ZnO exhibits uniform size distribution and a low tendency to form agglomerates [54, 55]. While active ZnO, which had more readily available Zn^{2+} , quickly reacted with the silica surface to form the covalent bond Si–O–Zn, protect the silica particles with a layer, and lessen the aggregation of filler in the matrix. Similarly, as shown in Figure 9, Octylamine modified ZnO formed the Si–O–Zn bonds and had a stronger affinity for the silica filler in F2BS. The filler-filler interaction was significantly reduced by an outer layer of octylamine and two layers covering the silica particles, resulting in a uniform distribution. This resulted in a lower filler-filler interaction and a low Payne effect. Compared to active ZnO, the available Zn sites were less in nano ZnO due to their lower surface area than active ZnO, resulting in a higher Payne effect than A2BS. C5BS had microsized conventional ZnO less available Zn sites reduced the dispersion in the matrix.

3.7. Mechanical characteristics of SBR/NR blends employing different ZnO

Table 5 lists the mechanical and physical properties obtained for the SBR/NR blends. The trend of the Payne effect was observed for the mechanical properties. As seen, the lower the Payne effect, the higher the polymer-filler interaction is, thereby improving the blends' mechanical properties; regarding the mechanical properties of silica-filled blends, functionalized ZnO as the activator exhibited the highest tensile strength and elongation at break compared to all other ZnO-filled blends. The higher reactivity of functionalized ZnO has been seen in the cure rate index analysis of the blends. A2BS had the second highest mechanical performance after F2BS; this could be due to the high reactivity of active ZnO to form an active-accelerator complex to react with sulfurating agents efficiently and increase the polymer-filler interaction. The lower particle size of nano ZnO increases the reactivity simultaneously, indicating a slight agglomeration at 2 phr loading, resulting in lower tensile strength and elongation at break than F2BS and A2BS. C5BS had lower tensile strength and elongation with a higher modulus due to its higher filler-filler interaction, lowering the mechanical performance of the blend as seen in the RPA analysis.

F2BS and A2BS silica-filled blends had the highest tensile strength and elongation at break, with increases

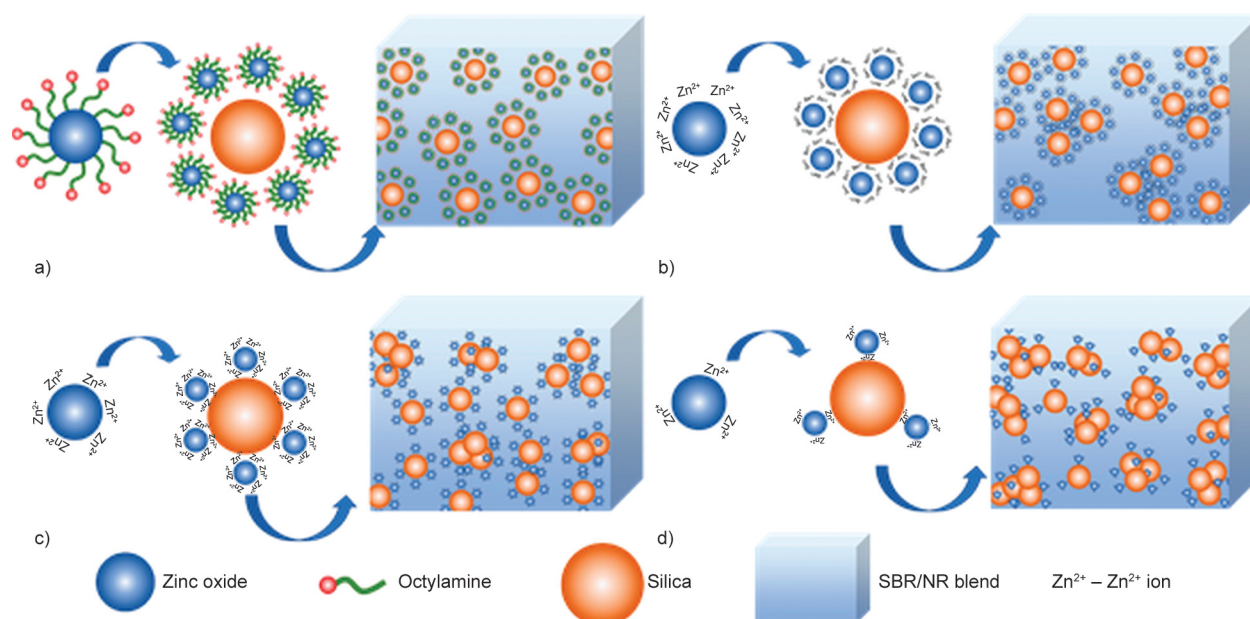


Figure 9. The proposed interaction of ZnO with silica particles in SBR/NR blends a) octylamine-modified ZnO in F2BS, b) active ZnO in A2BS, c) nano ZnO in N2BS, d) conventional ZnO in C5BS.

Table 5. Mechanical properties of SBR/NR blends.

Sample designation	Tensile strength [MPa]	Elongation at break [%]	Modulus at 300% [MPa]	Tear strength [N/mm]	Hardness [Shore A]
C5BS	15.1±2.4	362±61	12±1.2	85.0±3.4	68±1.3
A2BS	19.2±0.9	410±14	12.8±0.1	95.2±3.8	72±1.0
N2BS	15.5±2.4	351±49	12.7±0.4	74.1±2.1	68±1.8
F2BS	19.8±3.0	539±60	9.3±0.4	81.9±2.7	65±0.5

in tensile strength of 31% and elongation at break of 49% over C5BS. The highest tear strength was observed in A2BS among all the batches and had a 12% increase compared to C5BS. In terms of mechanical properties, active, nano, and functionalized ZnO at 2 phr were superior to conventional ZnO-loaded blends at 5 phr loading. The rubber compound's ZnO content is reduced by 60%, helping to lower the compound's cost and serving as a sustainable substitute additive to traditional ZnO.

3.8. Hot air accelerated aging study of SBR/NR blends with various ZnO

Figure 10 shows the crosslink density and mechanical property retention index of tensile strength, elongation at break and modulus values of silica-filled SBR/NR blends with various ZnO activators after accelerated aging study. The Equation (5) calculates the property retention index (*PRI*) [56]:

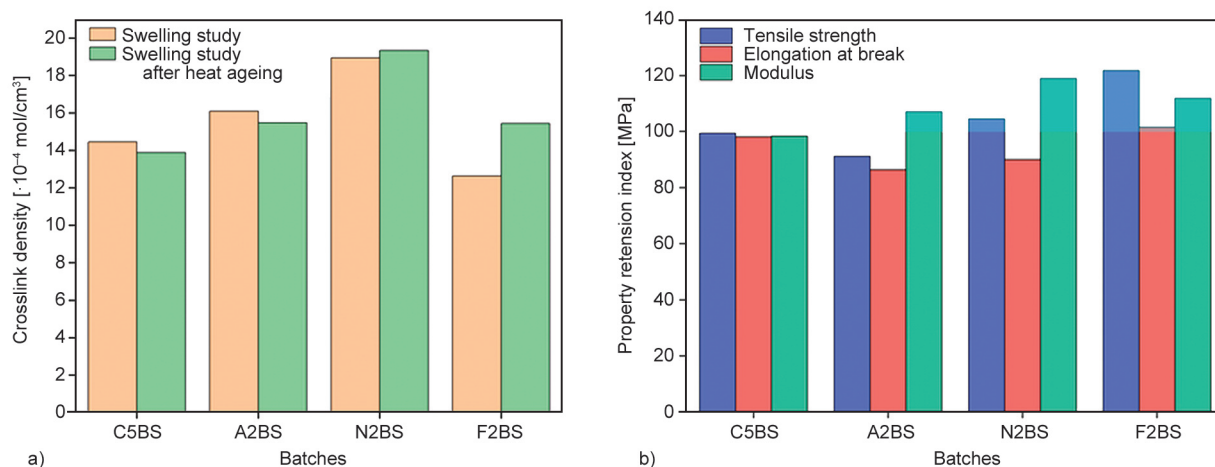
$$PRI [\%] = \frac{P}{P_0} \cdot 100 \quad (5)$$

where P_0 is mechanical properties of the blends before ageing, P the mechanical properties of the blends after ageing.

An increase in tensile strength was seen for F2BS and N2BS blends compared to C5BS, where the rise

in tensile strength after aging was prominent in F2BS. The F2BS was uniformly dispersed in the rubber blend in accordance with the mechanical properties obtained before and after aging [5]. This characteristic may also result from the increased crosslink density accompanying aging. The study reveals notable alterations in the crosslink density of F2BS and N2BS, signifying an increase, while the blends C5BS and A2BS exhibit a reduction in crosslink density after heat aging. These crosslink density fluctuations are directly correlated with the corresponding changes in the mechanical properties observed following the aging study.

Through the process of aging, the crosslink density of elastomer chains is augmented as pendant groups on the chains undergo reactions with neighboring pendant groups. This leads to the formation of additional crosslinks, resulting in an enhancement of tensile strength. N2BS also increased the tensile strength and modulus after heat aging due to their more stable mono- and disulfide crosslinks and higher crosslink density increased the resistance to thermal aging because of their stable structure [5, 57]. A2BS, N2BS, and F2BS showed increased modulus and decreased elongation following the aging process due to the increased molecular rigidity. The elastomer chains experience an increase in average molecular weight at

**Figure 10.** a) Crosslink density and b) mechanical properties of C5BS, A2BS, N2BS, and F2BS after thermal aging.

high crosslinking densities, which restricts the mobility of individual chain segments. As a result, the elastomeric substance stiffens, which reduces the elongation at break values [58, 59].

3.9. Field emission scanning electron microscopy (FESEM) of SBR/NR blends with various ZnO

The sulfur vulcanization's activation state and the SBR/NR blends' mechanical performance are greatly influenced by the ZnO activator and silica filler's dispersion state in the blend. The vulcanization efficiency decreases because of the ZnO activator particle aggregation, which reduces their contact surface and interactions with other crosslinking system modules. SEM and TEM were used to assess the dispersion level of different ZnO and silica fillers in the SBR/NR blends to investigate the morphology of the composites.

The morphological analysis of the blends was carried out using scanning electron microscopy, as shown in Figure 11 below, to support the Payne effect results. C5BS, A2BS, N2BS, and F2BS were analyzed for their relative dispersion in the blend. The grey area depicts the SBR/NR blend, and the white spherical particles indicate the filler and ZnO present in the matrix. In SBR/NR blends, the incorporation of octylamine ligands effectively prevented nanoparticle aggregation, leading to the uniform dispersion of F2BS with octylamine-modified ZnO nanoparticles [60].

The rate of agglomeration was observed in C5BS, N2BS and A2BS, respectively. In C5BS, the micron-sized conventional ZnO was less dispersed in the hydrophobic matrix due to its hydrophilic nature. Although, compared to transmission electron microscopy, distinguishing ZnO and silica in the matrix in SEM analysis was quite tricky.

To get a clearer picture of the distribution of elements in the matrix, we performed an EDS analysis at 20 μm scale. EDS spectrum and element mapping are given in Figure 12, and the atomic percentages of Si, O, and Zn have been provided. It has been observed that the atomic percentage of Si was 49% in F2BS, whereas in C5BS, it was 59%. It shows that the surface's layer formation of Si–O–Zn bonds has reduced the silica atomic % in the EDS spectrum.

3.10. Transmission electron microscopy of SBR/NR blends with various ZnO

The morphological changes in the bulk area of the SBR/NR blend system filled with highly dispersible silica at different ZnO activators can be determined from the TEM photomicrographs, as shown in Figure 13. In the C5BS blend, conventional ZnO with a cuboid structure was observed, along with silica particles in the SBR/NR blend, and it was discovered that the ZnO was not dispersed adequately within the matrix. To maintain consistency in the analysis, we used 100 nm-scale morphology images throughout the discussion section. The smaller particle size of nano ZnO leads to agglomeration in the blend, whereas active ZnO with more available Zn^{2+} readily reacted with the silica surface by forming the covalent bond Si–O–Zn and forming layer protection over the silica particles and reducing the aggregation of filler in the matrix. Similarly, using octylamine-modified ZnO had more affinity towards silica filler and formed the Si–O–Zn bonds, as shown in Figure 9. An outer layer of octylamine and two layers covering the silica particles drastically reduced the filler-filler interaction, resulting in uniform distribution [61]. Similar morphology was also observed in the SEM analysis. The SEM and TEM observations were in correlation with the obtained Payne effect.

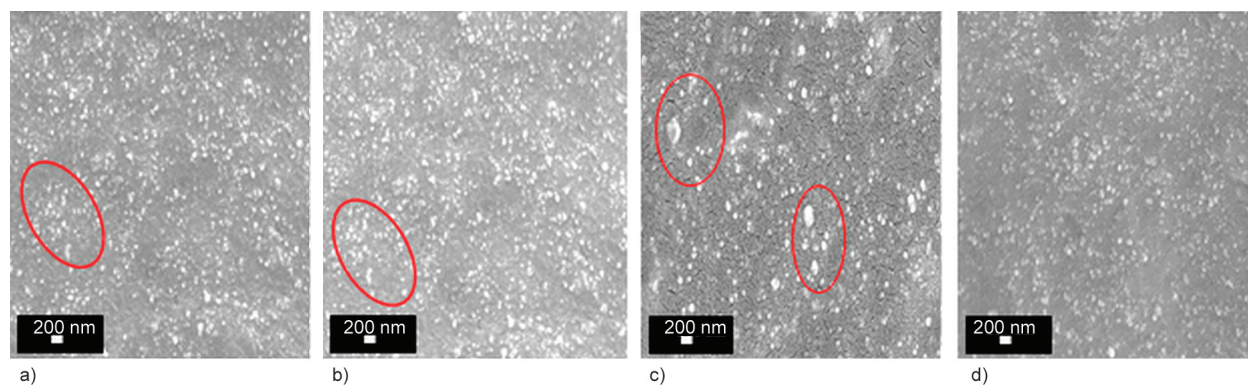


Figure 11. SEM images of a) C5BS, b) A2BS, c) N2BS, d) F2BS.

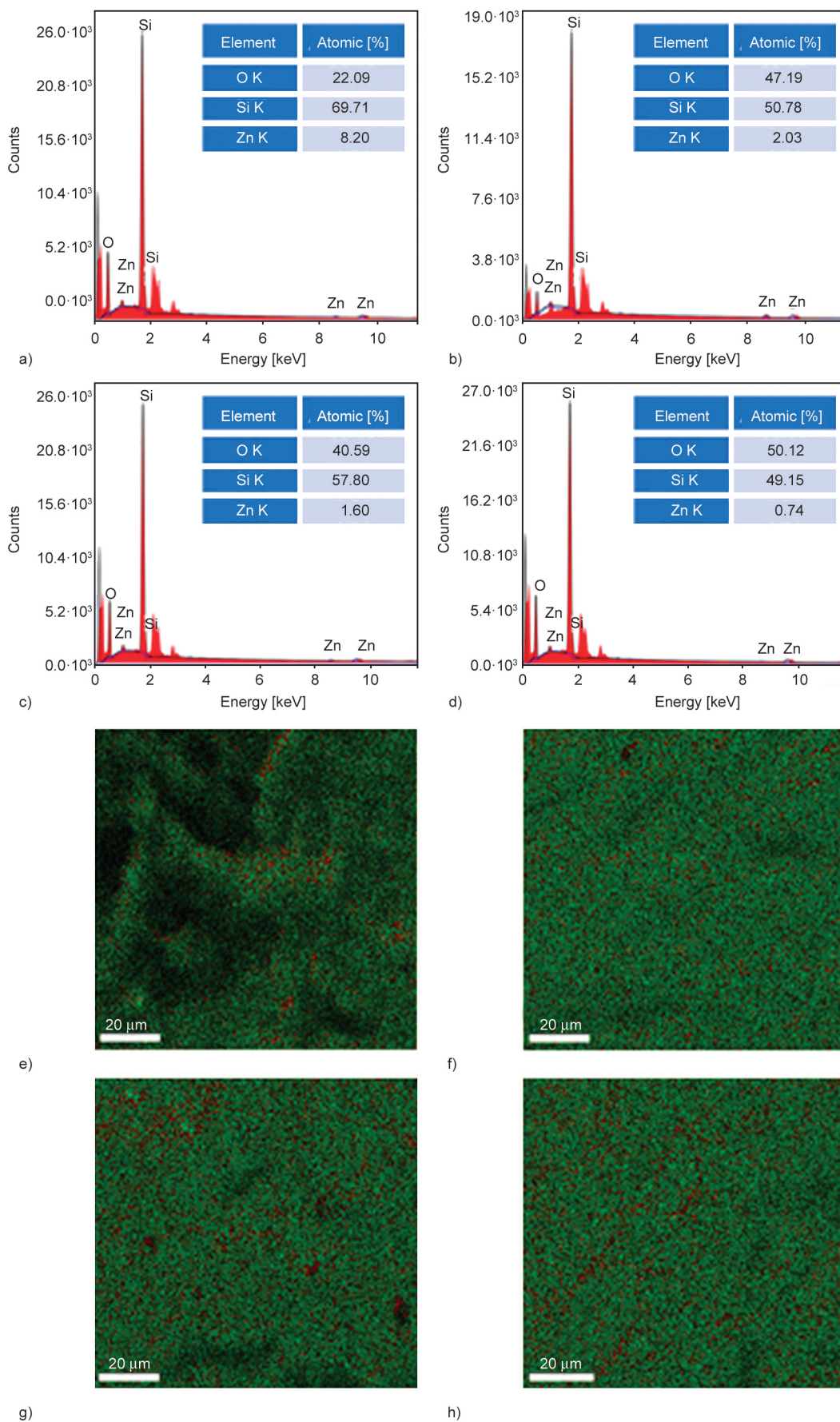


Figure 12. EDS spectrum of SBR/NR blends loaded with silica: a) C5BS, b) A2BS, c) N2BS, d) F2BS and EDX element mapping, e) C5BS, f) A2BS, g) N2BS, h) F2BS.

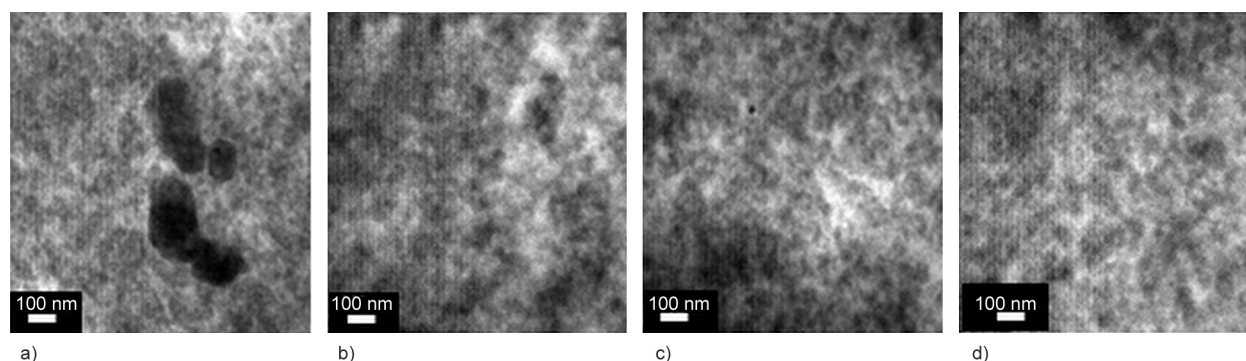


Figure 13. TEM images of SBR/NR blends loaded with silica: a) C5BS, b) A2BS, c) N2BS, d) F2BS.

4. Conclusions

This study focuses on replacing conventional ZnO with more sustainable activators such as octylamine-modified, active, and nano ZnO. It investigates the effect of these alternatives on the cure characteristics, temperature scanning stress relaxation, mechanical properties, dynamic mechanical properties, Payne effect, and morphology of SBR/NR blends filled with silica. When octylamine-modified ZnO (F2BS) and active ZnO (A2BS) were used, they interacted with the silica filler and formed a protective layer around the silica particles, as indicated by the results. The reduced aggregation between the filler particles resulted in better dispersion and 31% tensile strength, and 49% improvement in elongation at break compared to C5BS. In addition, active ZnO exhibited exceptional thermal stability. The Zn–O–Si interface peak was most pronounced in F2BS and A2BS, followed by N2BS, whereas C5BS exhibited a weaker intensity. This was further supported by the fact that C5BS exhibited a more significant Payne effect. A small amount of agglomeration resulted from the addition of nano ZnO at a loading of 2 phr. Higher delta torque, crosslink density, and stress values seen in the isothermal measurements of TSSR analysis suggest that nano ZnO had a significant effect as an activator on cure characteristics. The better filler dispersion resulted in the highest tear strength of A2BS, which improved over C5BS by 12%. At a loading of 5 phr, traditional ZnO-loaded blends had inferior mechanical properties to active, nano, and functionalized ZnO. With the use of nano, active, and octylamine-modified ZnO, the rubber compound by 60%, a sustainable alternative to traditional ZnO is provided that not only helps to reduce costs.

Acknowledgements

The authors express their gratitude to IPF Dresden, Germany, for offering the testing facility for TSSR and DMA analysis. They also extend their appreciation to Prof. Sven Weissner, Dr. Amit Das, and Mr. Subradeep Mandal for their valuable suggestions and collaboration throughout this research.

References

- [1] Mostoni S., D'Arienzo M., Di Credico B., Armelao L., Rancan M., Dirè S., Callone E., Donetti R., Susanna A., Scotti R.: Design of a Zn single-site curing activator for a more sustainable sulfur cross-link formation in rubber. *Industrial and Engineering Chemistry Research*, **60**, 10180–10192 (2021).
<https://doi.org/10.1021/acs.iecr.1c01580>
- [2] Alam M. N., Kumar V., Park S-S.: Advances in rubber compounds using ZnO and MgO as *co*-cure activators. *Polymers*, **14**, 5289 (2022).
<https://doi.org/10.3390/polym14235289>
- [3] Yasuda Y., Minoda S., Ohashi T., Yokohama H., Ikeda Y.: Two-phase network formation in sulfur crosslinking reaction of isoprene rubber. *Macromolecular Chemistry and Physics*, **215**, 971–977 (2014).
<https://doi.org/10.1002/macp.201400066>
- [4] Shaba E. Y., Jacob J. O., Tijani J. O., Suleiman M. A. T.: A critical review of synthesis parameters affecting the properties of zinc oxide nanoparticle and its application in wastewater treatment. *Applied Water Science*, **11**, 48 (2021).
<https://doi.org/10.1007/s13201-021-01370-z>
- [5] Lee Y. H., Cho M., Nam J-D., Lee Y.: Effect of ZnO particle sizes on thermal aging behavior of natural rubber vulcanizates. *Polymer Degradation and Stability*, **148**, 50–55 (2018).
<https://doi.org/10.1016/j.polymdegradstab.2018.01.004>
- [6] Rhodes E. P., Ren Z., Mays D. C.: Zinc leaching from tire crumb rubber. *Environmental Science and Technology*, **46**, 12856–12863 (2012).
<https://doi.org/10.1021/es3024379>

- [7] Liu X., Wang J., Ghenni A., ElGawady M. A.: Reduced zinc leaching from scrap tire during pavement applications. *Waste Management*, **81**, 53–60 (2018).
<https://doi.org/10.1016/j.wasman.2018.09.045>
- [8] Salvaggio A., Marino F., Albano M., Pecoraro R., Camiolo G., Tibullo D., Bramanti V., Lombardo B. M., Saccone S., Mazzei V., Brundo M. V.: Toxic effects of zinc chloride on the bone development in *Danio rerio* (Hamilton, 1822). *Frontiers in Physiology*, **7**, 153 (2016).
<https://doi.org/10.3389/fphys.2016.00153>
- [9] Raha S., Ahmaruzzaman M.: ZnO nanostructured materials and their potential applications: Progress, challenges and perspectives. *Nanoscale Advances*, **4**, 1868–1925 (2022).
<https://doi.org/10.1039/d1na00880c>
- [10] Wang Z., Hou Z., Liu X., Gu Z., Li H., Chen Q.: Preparation of zinc oxide with core–shell structure and its application in rubber products. *Polymers*, **15**, 2353 (2023).
<https://doi.org/10.3390/polym15102353>
- [11] Panampilly B., Thomas S.: Nano ZnO as cure activator and reinforcing filler in natural rubber. *Polymer Engineering and Science*, **53**, 1337–1346 (2013).
<https://doi.org/10.1002/pen.23383>
- [12] Sahoo S., Maiti M., Ganguly A., George J. J., Bhowmick A. K.: Effect of zinc oxide nanoparticles as cure activator on the properties of natural rubber and nitrile rubber. *Journal of Applied Polymer Science*, **105**, 2407–2415 (2007).
<https://doi.org/10.1002/app.26296>
- [13] Kim I.-J., Kim W.-S., Lee D.-H., Kim W., Bae J.-W.: Effect of nano zinc oxide on the cure characteristics and mechanical properties of the silica-filled natural rubber/butadiene rubber compounds. *Journal of Applied Polymer Science*, **117**, 1535–1543 (2010).
<https://doi.org/10.1002/app.31996>
- [14] Begum P. M. S., Yusuff K. K. M., Joseph R.: Preparation and use of nano zinc oxide in neoprene rubber. *International Journal of Polymeric Materials and Polymeric Biomaterials*, **57**, 1083–1094 (2008).
<https://doi.org/10.1080/00914030802341646>
- [15] Mottaghi M., Khorasani S. N., Esfahany M. N., Farzadfar A., Talakesh M. M.: Comparison of the effect of nano ZnO and conventional grade ZnO on the cross-linking densities of NR/BR and NR/SBR blends. *Journal of Elastomers and Plastics*, **44**, 443–451 (2012).
<https://doi.org/10.1177/0095244312439446>
- [16] Maiti M., Basak G. C., Srivastava V. K., Jasra R. V.: Influence of synthesized nano-ZnO on cure and physico-mechanical properties of SBR/BR blends. *International Journal of Industrial Chemistry*, **8**, 273–283 (2017).
<https://doi.org/10.1007/s40090-016-0107-7>
- [17] Sreethu T. K., Naskar K.: Zinc oxide with various surface characteristics and its role on mechanical properties, cure-characteristics, and morphological analysis of natural rubber/carbon black composites. *Journal of Polymer Research*, **28**, 183 (2021).
<https://doi.org/10.1007/s10965-021-02536-8>
- [18] Yang Z., Xie C.: Zn²⁺ release from zinc and zinc oxide particles in simulated uterine solution. *Colloids and Surfaces B: Biointerfaces*, **47**, 140–145 (2006).
<https://doi.org/10.1016/j.colsurfb.2005.12.007>
- [19] Vatanserver N., Polat Ş.: Effect of zinc oxide type on ageing properties of styrene butadiene rubber compounds. *Materials and Design*, **31**, 1533–1539 (2010).
<https://doi.org/10.1016/j.matdes.2009.09.015>
- [20] Sreethu T. K., Das M., Parathodika A. R., Bhattacharya A. B., Naskar K.: Understanding the role of ZnO as activator in SBR vulcanizates: Performance evaluation with active, nano, and functionalized ZnO. *Journal of Applied Polymer Science*, **140**, e53257 (2023).
<https://doi.org/10.1002/app.53257>
- [21] Sreethu T. K., Jana S., Jana N. R., Naskar K.: Influence of active, nano, and functionalized zinc oxide particles on the mechanical, cytotoxicity, and thermal stability of carbon black filled SBR/NR blends. *Polymer Engineering and Science*, **63**, 2354–2370 (2023).
<https://doi.org/10.1002/pen.26381>
- [22] Hong R., Pan T., Qian J., Li H.: Synthesis and surface modification of ZnO nanoparticles. *Chemical Engineering Journal*, **119**, 71–81 (2006).
<https://doi.org/10.1016/j.cej.2006.03.003>
- [23] Khurana N., Arora P., Pente A. S., Pancholi K. C., Kumar V., Kaushik C. P., Rattan S.: Surface modification of zinc oxide nanoparticles by vinyltriethoxy silane (VTES). *Inorganic Chemistry Communications*, **124**, 108347 (2021).
<https://doi.org/10.1016/j.inoche.2020.108347>
- [24] Rabin N. N., Morshed J., Akhter H., Islam M. S., Hossain M. A., Elias M., Alam M. M., Karim M. R., Hasnat M. A., Uddin M. N., Siddiquey I. A.: Surface modification of the ZnO nanoparticles with γ -aminopropyltriethoxysilane and study of their photocatalytic activity, optical properties and antibacterial activities. *International Journal of Chemical Reactor Engineering*, **14**, 785–794 (2016).
<https://doi.org/10.1515/ijcre-2015-0141>
- [25] Luo M., Shen C., Feltis B. N., Martin L. L., Hughes A. E., Wright P. F. A., Turney T. W.: Reducing ZnO nanoparticle cytotoxicity by surface modification. *Nanoscale*, **6**, 5791–5798 (2014).
<https://doi.org/10.1039/c4nr00458b>
- [26] Halbus A. F., Horozov T. S., Paunov V. N.: Surface-modified zinc oxide nanoparticles for antifungal and antiyeast applications. *ACS Applied Nano Materials*, **3**, 440–451 (2020).
<https://doi.org/10.1021/acsnm.9b02045>
- [27] Qin X., Xu H., Zhang G., Wang J., Wang Z., Zhao Y., Wang Z., Tan T., Bockstaller M. R., Zhang L., Matyjaszewski K.: Enhancing the performance of rubber with nano ZnO as activators. *ACS Applied Materials and Interfaces*, **12**, 48007–48015 (2020).
<https://doi.org/10.1021/acsmi.0c15114>

- [28] Presto D., Meyerhofer J., Kippenbrock G., Narayanan S., Ilavsky J., Moctezuma S., Sutton M., Foster M. D.: Influence of silane coupling agents on filler network structure and stress-induced particle rearrangement in elastomer nanocomposites. *ACS Applied Materials and Interfaces*, **12**, 47891–47901 (2020).
<https://doi.org/10.1021/acsami.0c12106>
- [29] Kumar A., Basu D., Sahoo S., Khanra S., Kumar N., Gonzalez M., Chattopadhyay S.: Green approaches for functionalized silica-based natural rubber nanocomposites using eco-friendly sodium alginate biopolymers for superior static and dynamic behaviors. *ACS Sustainable Chemistry and Engineering*, **11**, 6866–6878 (2023).
<https://doi.org/10.1021/acssuschemeng.2c06059>
- [30] Susanna A., Armelao L., Callone E., Dirè S., D’Arienzo M., Di Credico B., Giannini L., Hanel T., Morazzoni F., Scotti R.: ZnO nanoparticles anchored to silica filler. A curing accelerator for isoprene rubber composites. *Chemical Engineering Journal*, **275**, 245–252 (2015).
<https://doi.org/10.1016/j.cej.2015.04.017>
- [31] El-Refaie E. S. M., Nasrat L. S., Mohamed M. K., Ibrahim I. A.: Investigation the dielectric strength and mechanical features of nitrile butadiene rubber enhanced by different nanoparticles. *Egyptian Journal of Petroleum*, **32**, 11–17 (2023).
<https://doi.org/10.1016/j.ejpe.2023.03.001>
- [32] Pornprasit R., Pornprasit P., Boonma P., Natwichai J.: Determination of the mechanical properties of rubber by FT-NIR. *Journal of Spectroscopy*, **2016**, 4024783 (2016).
<https://doi.org/10.1155/2016/4024783>
- [33] Wang R., Xie C., Zeng L., Xu H.: Thermal decomposition behavior and kinetics of nanocomposites at low-modified ZnO content. *RSC Advances*, **9**, 790–800 (2019).
<https://doi.org/10.1039/c8ra09206k>
- [34] Movahed S. O., Ansarifar A., Mirzaie F.: Effect of various efficient vulcanization cure systems on the compression set of a nitrile rubber filled with different fillers. *Journal of Applied Polymer Science*, **132**, 41512 (2015).
<https://doi.org/10.1002/app.41512>
- [35] Franieck E., Fleischmann M., Hölck O., Kutuzova L., Kandelbauer A.: Cure kinetics modeling of a high glass transition temperature epoxy molding compound (EMC) based on inline dielectric analysis. *Polymers*, **13**, 1743 (2021).
<https://doi.org/10.3390/polym13111734>
- [36] Kamal M. R., Sourour S.: Kinetics and thermal characterization of thermoset cure. *Polymer Engineering and Science*, **13**, 59–64 (1973).
<https://doi.org/10.1002/pen.760130110>
- [37] Collard X., El Hajj M., Su B-L., Aprile C.: Synthesis of novel mesoporous ZnO/SiO₂ composites for the photodegradation of organic dyes. *Microporous and Mesoporous Materials*, **184**, 90–96 (2014).
<https://doi.org/10.1016/j.micromeso.2013.09.040>
- [38] Roy A., Polarz S., Rabe S., Rellinghaus B., Zähres H., Kruis F. E., Driess M.: First preparation of nanocrystalline zinc silicate by chemical vapor synthesis using an organometallic single-source precursor. *Chemistry – A European Journal*, **10**, 1565–1575 (2004).
<https://doi.org/10.1002/chem.200305397>
- [39] Susanna A., D’Arienzo M., Di Credico B., Giannini L., Hanel T., Grandori R., Morazzoni F., Mostoni S., Santambrogio C., Scotti R.: Catalytic effect of ZnO anchored silica nanoparticles on rubber vulcanization and cross-link formation. *European Polymer Journal*, **93**, 63–74 (2017).
<https://doi.org/10.1016/j.eurpolymj.2017.05.029>
- [40] Mostoni S., Milana P., D’Arienzo M., Dirè S., Callone E., Cepek C., Rubini S., Farooq A., Canevali C., Di Credico B., Scotti R.: Studying stearic acid interaction with ZnO/SiO₂ nanoparticles with tailored morphology and surface features: A benchmark for better designing efficient ZnO-based curing activators. *Ceramics International*, **49**, 24312–24321 (2023).
<https://doi.org/10.1016/j.ceramint.2022.12.013>
- [41] Ikeda Y., Yasuda Y., Ohashi T., Yokohama H., Minoda S., Kobayashi H., Honma T.: Dinuclear bridging bidentate zinc/stearate complex in sulfur cross-linking of rubber. *Macromolecules*, **48**, 462–475 (2015).
<https://doi.org/10.1021/ma502063m>
- [42] Yangthong H., Pichaiyut S., Wisunthorn S., Kummerlöwe C., Vennemann N., Nakason C.: Role of geopolymer as a cure activator in sulfur vulcanization of epoxidized natural rubber. *Journal of Applied Polymer Science*, **137**, 48624 (2020).
<https://doi.org/10.1002/app.48624>
- [43] Vennemann N.: Characterization of thermoplastic elastomers by means of temperature scanning stress relaxation measurements. in ‘Thermoplastic elastomers’ (ed.: El-Sonbati A. Z.) Intech, London, 347–370 (2016).
<https://doi.org/10.5772/35976>
- [44] Vennemann N., Schwarze C., Kummerlöwe C.: Determination of crosslink density and network structure of NR vulcanizates by means of TSSR. *Advanced Materials Research*, **844**, 482–485 (2014).
<https://doi.org/10.4028/www.scientific.net/AMR.844.482>
- [45] Parathodika A. R., Sreethu T. K., Maji P., Susoff M., Naskar K.: Influence of molecular and crosslink network structure on vulcanizate properties of EPDM elastomers. *Express Polymer Letters*, **17**, 722–737 (2023).
<https://doi.org/10.3144/expresspolymlett.2023.54>
- [46] Kim M. C., Adhikari J., Kim J. K., Saha P.: Preparation of novel bio-elastomers with enhanced interaction with silica filler for low rolling resistance and improved wet grip. *Journal of Cleaner Production*, **208**, 1622–1630 (2019).
<https://doi.org/10.1016/j.jclepro.2018.10.217>
- [47] Yang R., Song Y., Zheng Q.: Payne effect of silica-filled styrene-butadiene rubber. *Polymer*, **116**, 304–313 (2017).
<https://doi.org/10.1016/j.polymer.2017.04.003>

- [48] Khanra S., Sreenivasan P., Das S., Hore R.; Ganguly D., Chattopadhyay S.: Immobilization of a biobased process aid at the interface for binary silicone and fluoroelastomer based super specialty blends with silica for enhanced compatibility. *Journal of Materials Science*, **57**, 13974–13990 (2022).
<https://doi.org/10.1007/s10853-022-07504-1>
- [49] Ramier J., Gauthier C., Chazeau L., Stelandre L., Guy L.: Payne effect in silica-filled styrene-butadiene rubber: Influence of surface treatment. *Journal of Polymer Science Part B: Polymer Physics*, **45**, 286–298 (2007).
<https://doi.org/10.1002/polb.21033>
- [50] Bhattacharya M., Maiti M., Bhowmick A. K.: Influence of different nanofillers and their dispersion methods on the properties of natural rubber nanocomposites. *Rubber Chemistry and Technology*, **81**, 782–808 (2008).
<https://doi.org/10.5254/1.3548232>
- [51] Payne A. R.: The dynamic properties of carbon black-loaded natural rubber vulcanizates. Part I. *Journal of Applied Polymer Science*, **11**, 57–63 (1962).
<https://doi.org/10.1002/app.1962.070061906>
- [52] Li Y., Han B., Wen S., Lu Y., Yang H., Zhang L., Liu L.: Effect of the temperature on surface modification of silica and properties of modified silica filled rubber composites. *Composites Part A: Applied Science and Manufacturing*, **62**, 52–59 (2014).
<https://doi.org/10.1016/j.compositesa.2014.03.007>
- [53] Weber D., Botnaraş S., Pham D. V., Steiger J., De Cola L.: Functionalized ZnO nanoparticles for thin-film transistors: Support of ligand removal by non-thermal methods. *Journal of Materials Chemistry C*, **1**, 3098–3101 (2013).
<https://doi.org/10.1039/c3tc00576c>
- [54] Chang J., Waclawik E. R.: Experimental and theoretical investigation of ligand effects on the synthesis of ZnO nanoparticles. *Journal of Nanoparticle Research*, **14**, 1012 (2012).
<https://doi.org/10.1007/s11051-012-1012-4>
- [55] Verbakel F., Meskers S. C. J., Janssen R. A. J.: Surface modification of zinc oxide nanoparticles influences the electronic memory effects in ZnO-polystyrene diodes. *Journal of Physical Chemistry C*, **111**, 10150–10153 (2007).
<https://doi.org/10.1021/jp072999j>
- [56] Gujel A. A., Bandeira M., Giovanela M., Carli L. N., Brandalise R. N., Crespo J. S.: Development of bus body rubber profiles with additives from renewable sources: Part II – Chemical, physical-mechanical and aging characterization of elastomeric compositions. *Materials and Design*, **53**, 1119–1123 (2014).
<https://doi.org/10.1016/j.matdes.2013.07.102>
- [57] Pimolsiriphol V., Saeoui P., Sirisinha C.: Relationship among thermal ageing degradation, dynamic properties, cure systems, and antioxidants in natural rubber vulcanisates. *Polymer – Plastics Technology and Engineering*, **46**, 113–121 (2007).
<https://doi.org/10.1080/03602550601152861>
- [58] Takeoka Y., Liu S., Asai F.: Improvement of mechanical properties of elastic materials by chemical methods. *Science and Technology of Advanced Materials*, **21**, 817–833 (2020).
<https://doi.org/10.1080/14686996.2020.1849931>
- [59] Gotoh H., Liu C., Bin Imran A., Hara M., Seki T., Mayumi K., Ito K., Takeoka Y.: Optically transparent, high-toughness elastomer using a polyrotaxane cross-linker as a molecular pulley. *Science Advances*, **4**, eaat7629 (2018).
<https://doi.org/10.1126/sciadv.aat7629>
- [60] Mahmoodi N. M., Najafi F.: Preparation of surface modified zinc oxide nanoparticle with high capacity dye removal ability. *Materials Research Bulletin*, **47**, 1800–1809 (2012).
<https://doi.org/10.1016/j.materresbull.2012.03.026>
- [61] Bomila R., Venkatesan A., Srinivasan S.: Structural, luminescence and photocatalytic properties of pure and octylamine capped ZnO nanoparticles. *Optik*, **158**, 565–573 (2018).
<https://doi.org/10.1016/j.ijleo.2017.12.141>